

RAFM: Retrieval-Augmented Flow Matching for Unpaired CBCT-to-CT Translation

Xianhao Zhou¹, Jianghao Wu², Lanfeng Zhong^{1,3}, Ku Zhao¹, Jinlong He¹,
Shaoting Zhang^{1,3}, and Guotai Wang^{1,3*}

¹ School of Mechanical and Electrical Engineering,
University of Electronic Science and Technology of China, Chengdu, China

² Faculty of Information Technology,
Monash University, Melbourne, VIC 3800, Australia

³ Shanghai Artificial Intelligence Laboratory, Shanghai, China

Abstract. Cone-beam CT (CBCT) is routinely acquired in radiotherapy but suffers from severe artifacts and unreliable Hounsfield Unit (HU) values, limiting its direct use for dose calculation. Synthetic CT (sCT) generation from CBCT is therefore an important task, yet paired CBCT-CT data are often unavailable or unreliable due to temporal gaps, anatomical variation, and registration errors. In this work, we introduce rectified flow (RF) into unpaired CBCT-to-CT translation in medical imaging. Although RF is theoretically compatible with unpaired learning through distribution-level coupling and deterministic transport, its practical effectiveness under small medical datasets and limited batch sizes remains underexplored. Direct application with random or batch-local pseudo pairing can produce unstable supervision due to semantically mismatched endpoint samples. To address this challenge, we propose Retrieval-Augmented Flow Matching (RAFM), which adapts RF to the medical setting by constructing retrieval-guided pseudo pairs using a frozen DINOv3 encoder and a global CT memory bank. This strategy improves empirical coupling quality and stabilizes unpaired flow-based training. Experiments on SynthRAD2023 under a strict subject-level true-unpaired protocol show that RAFM outperforms existing methods across FID, MAE, SSIM, PSNR, and SegScore. The code is available at <https://github.com/HiLab-git/RAFM.git>.

Keywords: CBCT-to-CT translation · flow matching · rectified flow

1 Introduction

Computed tomography (CT) is the standard imaging modality for radiotherapy treatment planning because its Hounsfield Unit (HU) values provide reliable electron-density information for dose calculation [17]. In routine image-guided radiotherapy, cone-beam CT (CBCT) can be repeatedly acquired on treatment machines and is therefore valuable for adaptive radiotherapy workflows [3]. However, CBCT often suffers from severe artifacts and inaccurate HU values, which

* Corresponding author: Guotai Wang (guotai.wang@uestc.edu.cn).

limits its direct use for dose computation [13]. This has motivated CBCT-to-CT translation, i.e., synthesizing CT-like images from CBCT for downstream radiotherapy applications [17]. In practice, this problem is often inherently unpaired: paired CBCT–CT data are difficult to curate and align accurately, and even nominally paired scans may be affected by temporal gaps, anatomical variation, and registration errors. Thus, unpaired CBCT-to-CT translation is a practically important setting for improving CT-domain realism while preserving patient anatomy [7].

Existing unpaired CBCT-to-CT methods are mainly based on Generative Adversarial Networks (GANs) or diffusion/Schrödinger-bridge (SB) models. GAN-based methods, including cycle-consistent and contrastive variants [7, 1, 10], can produce strong visual results but inherit adversarial-training instability and sensitivity to architecture and loss balancing. Diffusion/SB-based methods have also shown promising performance in unpaired medical image translation [9, 4, 14], but typically require more complex training pipelines and may still involve adversarial components. These limitations motivate a fully non-adversarial alternative for anatomy-sensitive unpaired translation, where stable optimization and reliable structure preservation are particularly important.

Flow Matching and Rectified Flow (RF) provide a fully non-adversarial direction for unpaired translation by modeling it as deterministic transport between distributions [5, 6]. In RF, the training objective is defined on endpoint couplings whose marginals match the source and target domains, so it does not require voxel-aligned paired correspondences in principle [6]. Despite this appealing property, RF has not yet been systematically explored for medical image-to-image translation. A key practical challenge is that medical datasets are typically small, making finite-sample couplings a poor approximation of the desired distribution-level coupling; consequently, random or semantically arbitrary endpoint pairing can introduce noisy transport targets and harm anatomy-sensitive translation [11]. To mitigate transport noise, prior work in natural-image settings has proposed constructing couplings within each mini-batch to favor more compatible endpoints [18]. However, medical images are high-resolution and memory-intensive, so training often relies on small batch sizes, leaving batch-local coupling with an overly limited candidate pool and thus limited effectiveness.

To address these limitations, we introduce Retrieval-Augmented Flow Matching (RAFM), which enhances unpaired RF training through retrieval-guided coupling. RAFM retains the non-adversarial RF formulation while replacing random or batch-local pseudo pairing with global retrieval from a CT memory bank. Specifically, we use a frozen DINOv3 [15] encoder to construct a feature space for CT slices and retrieve a feature-similar CT slice for each CBCT slice to form pseudo endpoint pairs for flow matching. This retrieval-augmented strategy improves the empirical coupling quality under small-data, small-batch conditions while remaining strictly unpaired, as no subject identity or paired CBCT–CT correspondence is used. We evaluate RAFM on SynthRAD2023 under a strict subject-level true-unpaired protocol and demonstrate consistent improvements in image quality, distributional realism, and anatomy-related consistency.

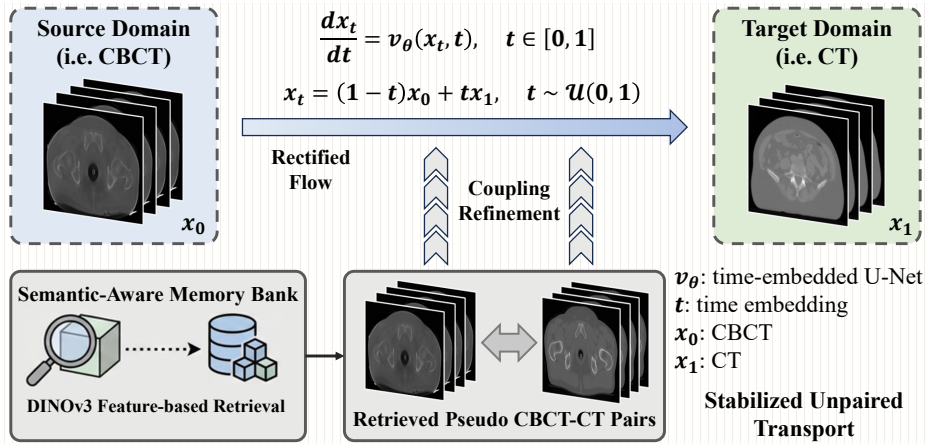


Fig. 1. Overview of Retrieval-Augmented Flow Matching (RAFM).

2 Method

2.1 Problem Setup and Overview

We consider unpaired CBCT-to-CT translation with two training sets, $\mathcal{D}_{\text{cbct}}^{\text{tr}} = \{x_i^{\text{cbct}}\}_{i \in \mathcal{A}}$ and $\mathcal{D}_{\text{ct}}^{\text{tr}} = \{x_i^{\text{ct}}\}_{i \in \mathcal{B}}$, where $\mathcal{A} \cap \mathcal{B} = \emptyset$. These two sets are sampled from the CBCT and CT marginals π_{cbct} and π_{ct} , respectively. Given $x^{\text{cbct}} \sim \pi_{\text{cbct}}$, the goal is to synthesize a CT-like slice \hat{x}^{ct} while preserving anatomy.

RAFM builds on Rectified Flow and formulates translation as deterministic transport from π_{cbct} to π_{ct} . In practice, under small-data and small-batch medical training, random or batch-local pseudo pairing often yields semantically mismatched endpoint pairs and noisy transport targets. To address this, RAFM retrieves, for each CBCT slice, a feature-similar CT slice from a global CT memory bank in a frozen feature space, thereby constructing a more consistent empirical coupling (Fig. 1).

2.2 Rectified Flow for Unpaired CBCT-to-CT Translation

The naive RF for image translation. Rectified Flow (RF) learns a time-dependent velocity field $v_\theta(x, t)$ and defines a deterministic transport ODE

$$\frac{dx_t}{dt} = v_\theta(x_t, t), \quad t \in [0, 1]. \quad (1)$$

In our setting, the transport starts from a CBCT sample and ends at a CT sample: $x_0 = x^{\text{cbct}} \sim \pi_{\text{cbct}}$ and $x_1 = x^{\text{ct}} \sim \pi_{\text{ct}}$. The scalar $t \in [0, 1]$ denotes the *transport time*, where $t = 0$ corresponds to the source endpoint x_0 and $t = 1$ corresponds to the target endpoint x_1 . RF constructs a linear interpolation path between endpoints and uses the intermediate state

$$x_t = (1 - t)x_0 + tx_1, \quad t \sim \mathcal{U}(0, 1), \quad (2)$$

as the input to the velocity network at time t . Along this straight path, the target instantaneous velocity is constant, $u_t = x_1 - x_0$, and RF trains v_θ by regressing to this target:

$$\mathcal{L}_{\text{RF}}(\theta) = \mathbb{E}_{(x_0, x_1) \sim \rho, t \sim \mathcal{U}(0,1)} \left[\|v_\theta(x_t, t) - (x_1 - x_0)\|_2^2 \right], \quad (3)$$

where ρ denotes an endpoint coupling used to sample (x_0, x_1) . Importantly, ρ does not need voxel-aligned CBCT–CT correspondences; it suffices that its marginals match the two data distributions [6]:

$$\rho_{x_0} = \pi_{\text{cbct}}, \quad \rho_{x_1} = \pi_{\text{ct}}. \quad (4)$$

Under this condition, RF learns the conditional mean velocity induced by ρ at each (x_t, t) , providing a fully non-adversarial way to transport π_{cbct} to π_{ct} via ODE integration at inference [5, 6].

Advantage and limitation of RF. For CBCT-to-CT translation, the goal is to correct CBCT-specific artifacts and HU bias while keeping patient anatomy unchanged. Rectified flow learns a deterministic ODE along the straight interpolation in Eq. (2), a formulation that has been repeatedly adopted for image-to-image translation where the output preserves the source content/structure while changing appearance or attributes [6, 21, 5]. In this sense, RF is *theoretically* compatible with the unpaired setting: the RF objective only requires an endpoint coupling ρ with correct marginals (Eq. (4)), rather than voxel-aligned paired correspondence. In practice, however, medical datasets are small and high-resolution training often forces very small mini-batches, so the empirical coupling induced by naive random pairing or batch-local matching can be a poor finite-sample approximation of the desired distribution-level coupling, leading to semantically mismatched endpoints and noisy transport targets [11, 18]. This motivates Sec. 2.3: we improve the practical coupling quality under small-data, small-batch conditions by introducing a global retrieval-based pseudo-pair construction strategy, which better realizes RF’s straight-line transport for anatomy-sensitive unpaired translation.

2.3 Retrieval-Augmented Flow Matching and Inference

CT slice memory bank construction. While standard RF permits arbitrary couplings with correct marginals, RAFM improves practical training by using global retrieval to construct a more reliable empirical coupling under limited medical data. We use a frozen DINOv3 [15] encoder $f(\cdot)$ to extract a class-token embedding $z = f(x) \in \mathbb{R}^d$ for each slice and maintain a fixed-capacity CT memory bank

$$\mathcal{M} = \{(z_j^{\text{ct}}, x_j^{\text{ct}})\}_{j=1}^K, \quad (5)$$

where z_j^{ct} is the DINOv3 feature for CT slice x_j^{ct} . Although the CT dataset is fixed, full-repository retrieval is inefficient in slice-wise training and may offer limited gains. Moreover, precomputing a single set of global features is less

general under data augmentation, where slice appearance (and thus features) may vary across iterations. To balance efficiency and coupling quality, we implement \mathcal{M} as a *rolling* (online FIFO) *training-global* buffer that aggregates CT slices across iterations. This bank is larger than a mini-batch but smaller than the full dataset, serving as a practical approximation to dataset-level retrieval. Concretely, each iteration enqueues CT feature–slice pairs from the current mini-batch into \mathcal{M} (FIFO when $|\mathcal{M}| > K$), and retrieves feature-similar CT slices for the CBCT mini-batch from the updated bank.

Retrieval-Augmented Flow Matching. For each CBCT slice x_i^{cbct} in the current mini-batch, we compute $z_i^{\text{cbct}} = f(x_i^{\text{cbct}})$ and retrieve the most similar CT slice from \mathcal{M} by cosine similarity, i.e., $j^* = \arg \max_j \cos(z_i^{\text{cbct}}, z_j^{\text{ct}})$. We then construct a pseudo endpoint pair $(x_0, x_1) = (x_i^{\text{cbct}}, x_{j^*}^{\text{ct}})$. The retrieved CT slice is selected from the target-domain memory bank solely by feature similarity, without using subject identity, temporal correspondence, registration, or paired CBCT–CT annotations. Therefore, RAFM remains a strictly unpaired framework. Feature similarity does not imply voxel-wise anatomical alignment, so the retrieved CT slice is used as an endpoint sample for coupling construction rather than a direct regression target.

The retrieval procedure induces a retrieval-based empirical coupling ρ_{retr} , which replaces random pairing or batch-local matching during training. Under this coupling, the RAFM objective is

$$\mathcal{L}_{\text{RAFMs}}(\theta) = \mathbb{E}_{(x_0, x_1) \sim \rho_{\text{retr}}, t \sim \mathcal{U}(0,1)} \left[\left\| v_\theta((1-t)x_0 + tx_1, t) - (x_1 - x_0) \right\|_2^2 \right]. \tag{6}$$

Compared with random or batch-wise pseudo pairing, retrieval-augmented pairing provides more semantically consistent transport supervision by expanding the candidate pool from the mini-batch to a global CT pool. We parameterize $v_\theta(x, t)$ using a time-conditioned U-Net [16]. At inference, given $x(0) = x^{\text{cbct}}$, we solve the learned ODE forward from $t = 0$ to $t = 1$ and take the final state as the synthesized CT slice \hat{x}^{ct} .

3 Experiments

3.1 Experimental Setup

We evaluate RAFMs on the SynthRAD2023 CBCT-to-CT benchmark (pelvis) [19], which contains 180 paired 3D cases. The dataset is split at the subject level into training/validation/test sets with a 7:1:2 ratio (126/18/36). To construct a strict true-unpaired setting, the 126 training subjects are further divided into two disjoint groups: CBCT volumes from 63 subjects and CT volumes from the remaining 63. Thus, no CBCT–CT correspondence or cross-modal subject overlap is available during training, while paired volumes are retained only for validation and testing. This subject-level protocol is stricter than slice-level shuffling.

Algorithm 1 Training of Retrieval-Augmented Flow Matching (RAFM)

-
- 1: **Input:** true-unpaired training sets $\mathcal{D}_{\text{cbct}}^{\text{tr}} = \{x_i^{\text{cbct}}\}_{i \in \mathcal{A}}$, $\mathcal{D}_{\text{ct}}^{\text{tr}} = \{x_i^{\text{ct}}\}_{i \in \mathcal{B}}$, where $\mathcal{A} \cap \mathcal{B} = \emptyset$, memory-bank size K
 - 2: **Initialize:** velocity network v_θ , frozen encoder f , empty CT memory queue \mathcal{M}
 - 3: **for** each training iteration **do**
 - 4: Sample a CBCT mini-batch $\{x_i^{\text{cbct}}\}_{i=1}^B$ from $\mathcal{D}_{\text{cbct}}^{\text{tr}}$
 - 5: Sample a CT mini-batch $\{x_m^{\text{ct}}\}_{m=1}^{B'}$ from $\mathcal{D}_{\text{ct}}^{\text{tr}}$
 - 6: Compute CT features $z_m^{\text{ct}} = f(x_m^{\text{ct}})$ for all m
 - 7: Enqueue $\{(z_m^{\text{ct}}, x_m^{\text{ct}})\}_{m=1}^{B'}$ into \mathcal{M} ; if $|\mathcal{M}| > K$, discard the oldest entries (FIFO)
 - 8: Initialize mini-batch loss $\mathcal{L} \leftarrow 0$
 - 9: **for** each x_i^{cbct} **do**
 - 10: Compute $z_i^{\text{cbct}} = f(x_i^{\text{cbct}})$
 - 11: Retrieve $x_{j^*}^{\text{ct}}$ from \mathcal{M} by cosine similarity:
 - 12: $j^* = \arg \max_j \cos(z_i^{\text{cbct}}, z_j^{\text{ct}})$
 - 13: Form pseudo pair $(x_0, x_1) \leftarrow (x_i^{\text{cbct}}, x_{j^*}^{\text{ct}})$
 - 14: Sample $t \sim \mathcal{U}(0, 1)$ and form $x_t = (1-t)x_0 + tx_1$
 - 15: $\mathcal{L} \leftarrow \mathcal{L} + \|v_\theta(x_t, t) - (x_1 - x_0)\|_2^2$
 - 16: **end for**
 - 17: $\mathcal{L} \leftarrow \mathcal{L}/B$
 - 18: Update θ using \mathcal{L}
 - 19: **end for**
-

We adopt slice-wise 2D training by decomposing each 3D volume into slices. All slices are resized to 256×256 , clipped to $[-1024, 2000]$, and normalized to $[-1, 1]$. The velocity field is parameterized by a time-conditioned U-Net with sinusoidal timestep embeddings and an MLP projection [16]. For RAFM, we use a frozen DINOv3-base encoder [15] for slice-level feature extraction and cosine-similarity retrieval in a CT memory bank (default $K = 512$, top-1). The model is trained with Adam (learning rate 2×10^{-4} , batch size 4) for 100 epochs. At inference, the learned ODE is solved using 10-step Euler integration.

For quantitative evaluation of the synthesized CT images, we report Mean Absolute Error (MAE), Structural Similarity (SSIM) [8], Peak Signal-to-Noise Ratio (PSNR) [8], Fréchet Inception Distance (FID) [2], and SegScore. SegScore is defined as the average Dice over pelvic organs segmented by TotalSegmentator [20] on synthesized and reference CT volumes. Unless otherwise specified, MAE/SSIM/PSNR/SegScore are computed on reconstructed 3D volumes, while FID is computed on 2D slices.

3.2 Results

We compare RAFM with representative unpaired CBCT-to-CT translation methods, including GAN-based methods (CycleGAN [7], GcGAN [1], CUT [10]) and diffusion/SB methods (SynDiff [9], UNSB [4]), under the same subject-level true-unpaired protocol.

As shown in Table 1, RAFM consistently outperforms prior unpaired methods under the subject-level true-unpaired protocol. Compared to the strongest base-

Table 1. Quantitative results on SynthRAD2023 for unpaired CBCT-to-CT translation. Best results are in bold. †denotes a significant improvement (p-value < 0.05) over existing method.

Method	MAE (HU)↓	SSIM (%)↑	PSNR (dB)↑	FID↓	SegScore (%)↑
CycleGAN [7]	173.8±14.2	77.96±0.78	23.57±1.62	99.75	64.03±1.98
GcGAN [1]	212.9±18.6	76.38±0.86	22.71±1.74	102.6	59.34±2.14
CUT [10]	109.0±12.1	80.27±0.62	24.47±1.28	66.77	70.49±1.58
SynDiff [9]	104.2±11.5	77.68±0.74	24.94±1.21	72.36	62.58±1.87
UNSB [4]	110.8±12.8	80.03±0.65	24.42±1.33	62.91	72.07±1.46
RAFM (ours)	101.2±10.4 †	80.96±0.49 †	25.15±1.12 †	53.29 †	75.77±1.21 †

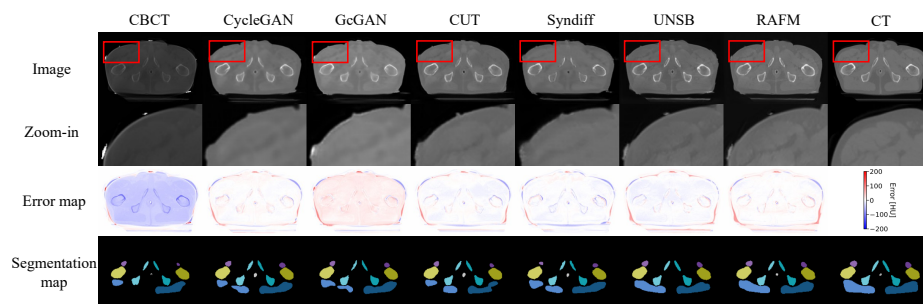


Fig. 2. Qualitative comparison on SynthRAD2023 for unpaired CBCT-to-CT translation.

lines, RAFM reduces MAE to 101.2 (vs. 104.2 for SynDiff and 110.8 for UNSB) and achieves the highest SSIM/PSNR (80.96% and 25.15). Notably, RAFM yields the best distributional realism with the lowest FID (53.29), improving over UNSB (62.91) and CUT (66.77). It also improves anatomy-related consistency, reaching a SegScore of 75.77%, significantly outperforming UNSB (72.07%) and CUT (70.49%). Qualitative examples in Fig. 2 further show cleaner artifact suppression and more stable anatomical structures achieved by our method than the others. In terms of computational cost, RAFM trains a single forward CBCT→CT transport model, with training overhead comparable to a standard time-conditioned U-Net, avoiding the doubled generators and cycle-consistency constraints required by bidirectional frameworks such as CycleGAN [7] and SynDiff [9]. At inference, RAFM uses only 10 ODE steps, making it substantially faster than multi-step diffusion sampling, while remaining within a practical runtime range compared to GAN-based baselines.

3.3 Ablation Study

We conduct a unified ablation to study coupling quality and candidate-pool size in true-unpaired training. We compare: (i) a conventional unpaired regression baseline (vanilla U-Net [12] without flow matching), (ii) RF with random

Table 2. Unified ablation on coupling strategy and candidate-pool size K on SynthRAD2023. $K=0$ denotes random coupling and $K=4$ denotes batch-wise matching; paired RF is shown as a reference (upper bound).

Training strategy	K	MAE (HU)↓	SSIM (%)↑	PSNR (dB)↑	FID↓	SegScore (%)↑
Vanilla U-Net (w/o FM)	0	127.1	67.70	23.01	209.8	1.45
RF + random coupling	0	132.2	77.20	23.76	96.15	74.27
RF + batch-wise matching	4	118.4	79.84	24.41	71.32	75.01
RAFM	256	109.2	80.46	24.75	53.74	75.34
RAFM	512	101.2	80.96	25.15	53.29	75.77
RAFM	1024	98.50	80.68	25.15	55.41	75.29
RAFM	4096	103.0	80.81	25.11	58.06	74.94
Paired RF (upper bound)	/	72.28	86.30	27.12	59.78	76.87

unpaired coupling, (iii) RF with batch-wise matching, and (iv) RAFM with retrieval-augmented coupling using different memory-bank sizes. For a unified view, random coupling is treated as the degenerate case with no retrieval pool ($K = 0$), and batch-wise matching is treated as a local strategy with candidate pool size equal to the mini-batch size ($K = 4$). We also report a paired RF model trained with full paired CBCT-CT supervision as a supervised reference (upper bound).

Table 2 shows a clear performance improvement as coupling quality and candidate-pool size increase. The vanilla U-Net baseline (w/o FM) fails under true-unpaired supervision (FID 209.8, SegScore 1.45%), confirming that direct regression to arbitrary targets is ineffective. In contrast, RF remains robust even with random coupling (FID 96.15, SegScore 74.27%), and batch-wise matching ($K=4$) further improves MAE and FID. By enlarging the candidate pool beyond the mini-batch, RAFM consistently outperforms local matching and achieves the best true-unpaired trade-off at $K=512$ (MAE 101.2, FID 53.29, SegScore 75.77%), with diminishing returns for larger banks. Paired RF provides an upper bound on voxel-wise fidelity (MAE 72.28, SSIM 86.30%), while RAFM remains close in anatomy-related metrics (SegScore 75.77% vs. 76.87%), indicating that semantically meaningful coupling enables stable anatomy preservation even without paired supervision.

4 Conclusion

We proposed Retrieval-Augmented Flow Matching (RAFM), a non-adversarial rectified-flow framework for unpaired CBCT-to-CT translation with retrieval-augmented coupling. Using a frozen DINOv3 encoder and a global CT memory queue, RAFM constructs more reliable pseudo pairs than random or batch-local matching under small-data, small-batch training. Experiments on SynthRAD2023 with a strict subject-level true-unpaired protocol demonstrate strong image quality and anatomy consistency, and ablations highlight coupling quality as a key factor for narrowing the gap to paired rectified-flow training.

References

1. Fu, H., Gong, M., Wang, C., Batmanghelich, K., Zhang, K., Tao, D.: Geometry-consistent generative adversarial networks for one-sided unsupervised domain mapping. In: Proceedings of the IEEE/CVF conference on computer vision and pattern recognition. pp. 2427–2436 (2019)
2. Heusel, M., Ramsauer, H., Unterthiner, T., Nessler, B., Hochreiter, S.: Gans trained by a two time-scale update rule converge to a local nash equilibrium. *Advances in neural information processing systems* **30** (2017)
3. Horner, K., O’Malley, L., Taylor, K., Glenny, A.M.: Guidelines for clinical use of CBCT: a review. *Dentomaxillofacial radiology* **44**(1), 20140225 (2015)
4. Kim, B., Kwon, G., Kim, K., Ye, J.C.: Unpaired image-to-image translation via neural schrödinger bridge. In: 12th International Conference on Learning Representations, ICLR 2024 (2024)
5. Lipman, Y., Chen, R.T., Ben-Hamu, H., Nickel, M., Le, M.: Flow matching for generative modeling. arXiv preprint arXiv:2210.02747 (2022)
6. Liu, X., Gong, C., Liu, Q.: Flow straight and fast: Learning to generate and transfer data with rectified flow. arXiv preprint arXiv:2209.03003 (2022)
7. Liu, Y., Lei, Y., Wang, T., Fu, Y., Tang, X., Curran, W.J., Liu, T., Patel, P., Yang, X.: CBCT-based synthetic CT generation using deep-attention cyclegan for pancreatic adaptive radiotherapy. *Medical physics* **47**(6), 2472–2483 (2020)
8. Müller-Franzes, et al., G.: A multimodal comparison of latent denoising diffusion probabilistic models and generative adversarial networks for medical image synthesis. *Scientific Reports* **13**(1), 12098 (2023)
9. Özbey, M., Dalmaz, O., Dar, S.U., Bedel, H.A., Öztürk, Ş., Güngör, A., Cukur, T.: Unsupervised medical image translation with adversarial diffusion models. *IEEE Transactions on Medical Imaging* **42**(12), 3524–3539 (2023)
10. Park, T., Efros, A.A., Zhang, R., Zhu, J.Y.: Contrastive learning for unpaired image-to-image translation. In: European conference on computer vision. pp. 319–345. Springer (2020)
11. Reu, T., Dromigny, S., Bronstein, M., Vargas, F.: Gradient variance reveals failure modes in flow-based generative models. arXiv preprint arXiv:2510.18118 (2025)
12. Ronneberger, O., Fischer, P., Brox, T.: U-Net: Convolutional networks for biomedical image segmentation. In: MICCAI. pp. 234–241 (2015)
13. Schulze, R., Heil, U., Groß, D., Bruellmann, D.D., Dranischnikow, E., Schwanecke, U., Schoemer, E.: Artefacts in CBCT: a review. *Dentomaxillofacial Radiology* **40**(5), 265–273 (2011)
14. Shi, K., Ouyang, S., Liu, G., Luo, Y., Su, K., Liang, Z., Du, B.: Anatomy-conserving unpaired cbct-to-ct translation via schrödinger bridge. In: International Conference on Medical Image Computing and Computer-Assisted Intervention. pp. 46–55. Springer (2025)
15. Siméoni, et al., O.: Dinov3. arXiv preprint arXiv:2508.10104 (2025)
16. Song, Y., Sohl-Dickstein, J., Kingma, D.P., Kumar, A., Ermon, S., Poole, B.: Score-based generative modeling through stochastic differential equations. arXiv preprint arXiv:2011.13456 (2020)
17. Spadea, M.F., Maspero, M., Zaffino, P., Seco, J.: Deep learning based synthetic-CT generation in radiotherapy and PET: a review. *Medical physics* **48**(11), 6537–6566 (2021)
18. Stoica, G., Ramanujan, V., Fan, X., Farhadi, A., Krishna, R., Hoffman, J.: Contrastive flow matching. In: Proceedings of the IEEE/CVF International Conference on Computer Vision. pp. 1185–1194 (2025)

19. Thummerer, A., van der Bijl, E., Galapon Jr, A., Verhoeff, J.J., Langendijk, J.A., Both, S., van den Berg, C.N.A., Maspero, M.: Synthrad2023 grand challenge dataset: Generating synthetic CT for radiotherapy. *Medical physics* **50**(7), 4664–4674 (2023)
20. Wasserthal, et al., J.: Totalsegmentator: robust segmentation of 104 anatomic structures in CT images. *Radiology: Artificial Intelligence* **5**(5), e230024 (2023)
21. Zhu, Y., Zhao, W., Li, A., Tang, Y., Zhou, J., Lu, J.: Flowie: Efficient image enhancement via rectified flow. In: *Proceedings of the IEEE/CVF Conference on Computer Vision and Pattern Recognition*. pp. 13–22 (2024)